External noise in semiconductor lasers

Javier M. Buldú[a], J. García-Ojalvo[a], M.C. Torrent[a], J.M. Sancho [b], Claudio R. Mirasso[c] and Dante Chialvo[d]

[a] Departament de Física i Enginyeria Nuclear, Universitat Politècnica de Catalunya, Colom 11, E-08222 Terrassa, Spain
[b] Departament d'Estructura i Constituents de la Matèria, Universitat de Barcelona, Diagonal 647, E-08028 Barcelona, Spain
[c]Departament de Física, Universitat de les Illes Balears, E-07071 Palma de Mallorca, Spain
[d] Department of Physiology, Northwestern University, Chicago, IL 60611, USA

ABSTRACT

In the present work we review recent results concerning stochastic phenomena in semiconductor lasers with optical feedback which operate in the low-frequency fluctuation (LFF) regime. Under these conditions the output intensity of the laser shows an irregular pulsated behavior in the form of sudden intensity dropouts. In the first two sections we show numerically the existence of stochastic and coherence resonance in the dropout appearance. These resonances are caused by the help of external colored noise introduced through the pumping current of the laser. In the third section we describe a recently reported new type of stochastic resonance, where a nonlinear system shows a resonance at a frequency not present neither at its internal time scales nor at any external perturbation. This phenomenon, known as ghost resonance, is reported both numerically and experimentally.

Keywords: external noise, coherence resonance, stochastic resonance, ghost resonance.

1. STOCHASTIC RESONANCE IN SEMICONDUCTOR LASERS

1.1. Helping modulation with noise

Noise has always been considered as a source of disorder and therefore its presence in any dynamical system has been undesirable. Nevertheless, over the last two decades, the studies of how noise can give order to a system have attracted the interest of many researches.[1,2] Particularly, stochastic resonance (SR)[3,4] has been observed in many different fields like biological systems,[5–7] electronic circuits[8–10] or optical systems.[11–13] SR can be defined as an enhancement of the regularity of a system output for certain range of noise amplitudes when the system is driven by a weak periodic signal. In fact, the system is helped by noise to follow the frequency of the periodic signal in a resonance-like behavior. When the noise amplitude is not high enough to produce any effect at the system output, or when it is too high that it overtakes the dynamics of the system, no regularity or entrainment will be observed. Only for intermediate values of noise its effect will be sufficient to help the system to follow the weak periodic driving without having a too noisy output.

The concept of SR was introduced by Benzi *et al.*[3] in order to explain the periodicity observed in the ice ages. Since the work of Benzi *et al.*, SR has been observed in many dynamical systems, some of them quite different in nature. Although, in all cases, the results obtained show a constructive interplay between noise and a weak periodic signal, the mechanism underlying the SR can be different depending on the nature of the system. In this sense, several studies have shown that the mechanism of SR can be explained with different theoretical models. Among all of them, the double-well and the excitable systems have been the most studied (see[4] for an overview of the different SR mechanisms).

In the current section we will focus in the SR phenomenon in a system with excitability properties. This kind of systems have only one stable state, from which the system can depart if an external perturbation above a

Further author information: (Send correspondence to J.M.B.)
J.M.B.: E-mail: javier.martin-buldu@upc.es, Telephone: +34 93 739 8948
J.G.O.: E-mail: jordi.g.ojalvo@upc.es, Telephone: +34 93 739 8645

Fluctuations and Noise in Photonics and Quantum Optics II, edited by Peter Heszler, Derek Abbott, Julio R. Gea-Banacloche, Philip R. Hemmer, Proceedings of SPIE Vol. 5468 (SPIE, Bellingham, WA, 2004) 0277-786X/04/$15 · doi: 10.1117/12.546743

certain threshold is applied. After the excursion, the system returns to the initial stable state after a deterministic time.

The system studied consists on a semiconductor laser with optical feedback in the low-frequency fluctuation regime which has been seen to have similar characteristics to excitable systems.[14,15] In this regime, the laser output exhibits intensity drops at irregular times ($\sim$ tens of nanoseconds), which in fact are the envelope of even faster optical pulses ($\sim$ tens of picoseconds). Due to the relation between frequencies of the fast optical pulses and the dropouts of the intensity envelope, the later were called low-frequency fluctuations (LFF). In Fig. 1(a) we can see a typical time trace of the output intensity of the laser in the LFF regime. The signal has been filtered with a 500 MHz filter in order to reproduce the response obtained from a typical photodetector although, in fact this is just the envelope of the real laser intensity, which is displayed without filtering in Fig. 1(b) [note the time scale difference]. Comparing the intensity dropouts of the filtered intensity, with the fast pulses of the real intensity ($\sim$ 100 ps wide) it is clear why they are called low-frequency fluctuations.

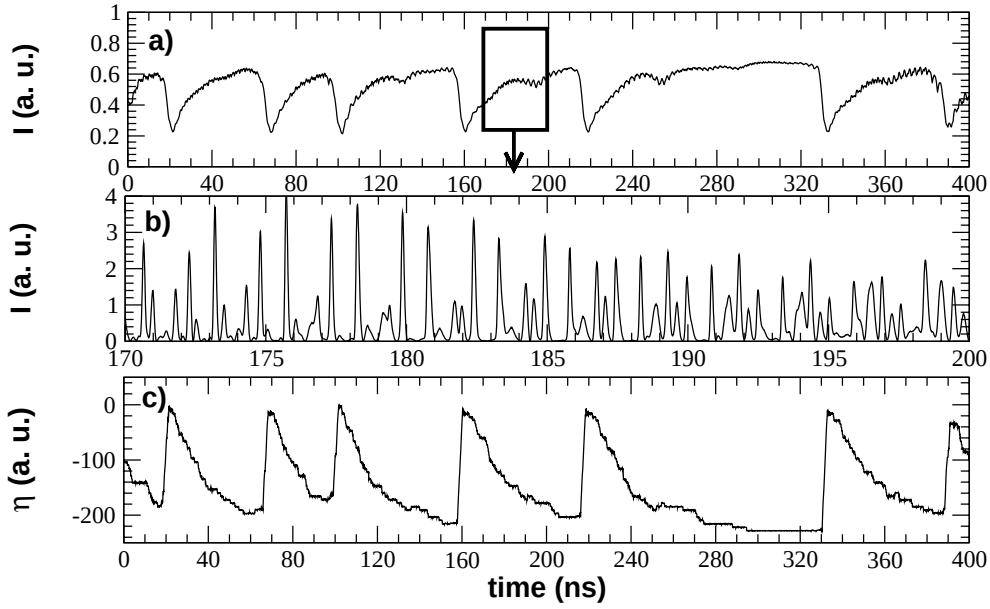

Figure 1. Numerical results obtained with the Lank-Kobayashi rate equations, showing the evolution of the output intensity in the LFF regime. In (a), the intensity has been 500 MHz filtered with a fourth-order Butterworth filter in order to simulate the behavior of a typical photodetector. In (b), the intensity has been not filtered allowing to observe the fast (real) intensity pulses emitted by the laser in the LFF regime (note the difference in the time scale). In (c) we plot the carrier number [N(t)] and in (d) the phase difference $\eta(t) = \phi(t) - \phi(t-\tau)$.

In Fig. 1(c) we display the evolution of an interesting variable of the system, the phase difference between the field that is leaving the laser facet and the field arriving from the external mirror, which is defined as $\eta(t) = \phi(t) - \phi(t-\tau)$. By comparing Fig. 1(a) and Fig. 1(c) can observe how the intensity dropouts are related with an increase of η to zero, while the intensity recovery is reflected in the phase difference as a decrease towards a negative given value. Numerically, to detect a dropout it is more practical to analyze the behavior of the phase difference $\eta(t)$, since its variation is smoother than that of the intensity, and easier to characterize. Therefore a dropout occurrence is recorded when the phase difference suddenly increases in a fixed large amount (e.g. 12π in our case).[15]

Marino *et al.*[16] experimentally observed that it was possible to entrain the appearance of the intensity dropouts with an external periodic signal when an adequate amount of noise was introduced through the pumping current of the laser. This entrainment due to noise is an evidence of the SR phenomenon and will be numerically studied in the present section. The analysis will be performed in the framework of the Lang-Kobayashi[17] (LK) model, where the pumping term has been modified in order to introduce periodic and noisy signals. Being $E(t)$

the temporal evolution of the slowly varying complex envelope of the electric field and $N(t)$ the excess carrier number, the dimensionless form of the model reads:

$$\frac{dE}{dt} = \frac{1+i\alpha}{2}[G(|E|^2,N)-\gamma]\,E(t) + \kappa e^{-i\omega\tau_f}E(t-\tau_f) + \sqrt{2\beta N}\zeta(t) \quad (1)$$

$$\frac{dN}{dt} = C(t) - \gamma_e N(t) - G(|E|^2,N)\,|E(t)|^2 \quad (2)$$

where γ and γ_e are respectively the inverse lifetimes of photons and carriers, α is the linewidth enhancement factor, and ω is the free running lasing frequency. The pumping term $C(t)$ has the form $C(t) = C_0[1+\xi(t)+A\sin(\Omega t)]$, where C_0 is the bias pumping rate (directly related to the DC driving current; $C_0 = \gamma_e N_{th}/e$ is the solitary-laser threshold), and which is affected by a random term [represented by $\xi(t)$] and a harmonic driving of amplitude A and frequency Ω. The last term in the electric-field equation [Eq.(1)] represents spontaneous emission fluctuations, with $\zeta(t)$ given by a Gaussian white noise of zero mean and unity intensity, and β measuring the internal noise strength. The material-gain function $G(|E|^2,N)$ is given by:

$$G(|E|^2,N) = \frac{g_N(N(t)-N_0)}{1+s|E(t)|^2}\,, \quad (3)$$

where g_N is the differential gain coefficient, N_0 is the carrier number in transparency and s the saturation coefficient. The threshold carrier number is $N_{\rm th} = \gamma/g_N + N_0$. Finally the optical feedback term is described by two parameters: the feedback strength κ and the external round–trip time τ_f. We set the laser parameters to the values presented in Table 1 of Appendix A.

Special care must be taken when introducing external noise into the system. At this point, it is important to recall the fast pulsated dynamics ($\sim$ tens of picoseconds)[18,19] of the intensity output in the LFF regime. Therefore, it would not be realistic to assume external white noise, for the simple reason that it is not possible to reach experimentally. The bandwidth limitations of the electronics involved and the fast dynamics of the laser intensity will lead to an external noise with non-negligible correlation time. Hence, the noise term $\xi(t)$ in our model is taken to be a time-correlated Gaussian random process of the Ornstein-Uhlenbeck type, with zero mean and correlation

$$\langle \xi(t)\xi(t')\rangle = \frac{D}{\tau_c}\,e^{-(t-t')/\tau_c}\,. \quad (4)$$

This external noise is characterized by two parameters, its intensity D and its correlation time τ_c. The variance of the noise is given by D/τ_c, and hence we will measure its amplitude as $\sigma = \sqrt{D/\tau_c}$.

Applying the SR concept to our system, we modulate the laser with a weak external signal, while it is operating in the LFF regime. Later on we force the intensity dropouts to follow the modulation signal just by applying the right amount of noise. External noise will be introduced to the system through the injection current of the laser. In Fig. 2 we show the numerical intensity (top plots) and phase difference (bottom plots) time traces with their corresponding probability distribution function (PDF) of the time between dropouts for three different values of the noise amplitude ($\sigma = \sqrt{D/\tau_c}$). We initially set the modulation amplitude to 3% of the threshold current (A=0.03) and the modulation period at $T = 70$ ns. The noise correlation time is fixed to $\tau_c = 240$ ps, since this value has been shown to be optimal for coherence resonance in the same system.[20] In the absence of noise [Fig. 2(a)], and with these parameters, the PDF presents two peaks at periods around 70 ns and 140 ns, which are multiples of the modulation period. When noise intensity is increased to intermediate values, $D = 0.3$ ps, it can be seen just one peak in the PDF, centered at $\sim$ 70 ns, i.e. at the modulation period [Fig. 2(b)]. If noise intensity is further increased the system loses the regularity, and dropouts fall at lower intervals, were LFF are difficult to observe [Fig. 2(c)].

Hence Fig. 2 displays the main characteristics of SR, namely that for a certain range of noise intensities the interval between dropouts follows the modulation period, showing a peak in the PDF at $t \simeq 70$ ns. As a consequence we can say that noise not only helps the system to follow a weak driving but also gives regularity to the dropout time series. This enhancement of the LFF regularity is observed in Fig. 3 (left plots), where the standard deviation of dropout periods (bottom plot) and the mean period (top plot) are shown for different noise intensities. A minimum at noise intensity $D = 0.25$ ps can be observed, which implies the maximum regularity of

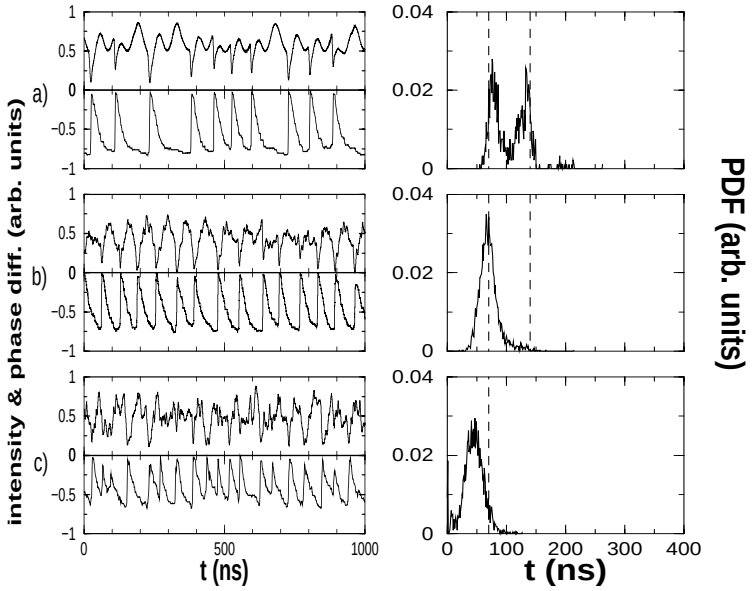

Figure 2. Time evolution of the laser intensity (left column, top plots), the phase difference $\eta(t)$ (left column, bottom plots) and the corresponding PDFs (right column) of the interval between dropouts for increasing values of the external noise strength D. (a) $D = 0.0$ ps (b) $D = 0.3$ ps (c) $D = 0.8$ ps. Noise correlation time is set to $\tau_c = 240$ ps. Parameters of the model are detailed in Appendix A.

the intensity dropouts. But the main point of the stochastic entrainment is that the mean value of the dropout periods for the maximum regularity ($D = 0.25$ ps) is the modulation period, $T = 70$ ns. Thus, we observe that noise helps the system to respond to the external forcing when the system is not able by itself (due to the weakness of the modulation signal), a typical feature of SR.

In Fig. 3 (right plot) we also present the PDFs obtained for increasing values of the noise intensity. When analyzing the evolution of the maximum values of the PDF in each plot we observe, for a noise intensity $D = 0.0$ ps, two peaks located at periods T and 2T. This means that modulation is not strong enough to force the system to follow its period, a fact that would be possible if modulation amplitude were increased. Although the system is not able to follow the modulation amplitude it is clear that the dynamics is dominated by the modulation, since we see the two peaks at T and 2T. When noise is increased up to $D = 0.25$ ps, the system response to the modulation is increased. At this moment, noise plays a constructive role and helps modulation to control the output dynamics. If noise intensity is further increased, the peak in the PDF moves to lower periods and diminishes. This movement towards shorter intervals between dropouts is the consequence that noise dominates the dynamics of the system in front of the modulation, as it can also be seen in Fig. 2(c).

1.2. Noise correlation time and stochastic resonance

Once the effect of the noise intensity is understood, let us study the effect of the noise correlation time in the system. From Eq.(4), there are two parameters of the noise that can be controlled: the noise intensity D and the correlation time τ_c. From these parameters we obtain the noise amplitude σ. From now on, the value of σ is fixed to 0.035 and τ_c is increased from few picoseconds to thousands of nanoseconds, in order to study its effect in the dropout regularity. As we have mentioned, time-correlated noise must be considered due to experimental limitations and the fast dynamics involved in the system and, as we will see, the value of noise correlation τ_c will be a crucial parameter.[20] In Fig. 4 we present time traces for three different correlation times together with the corresponding PDFs. The results obtained are qualitatively the same as those obtained when noise intensity was increased. An improvement of the system response to the modulation is observed when $\tau_c \sim 200$ ps, which allows us to conclude that the SR is also observed for a particular value of the noise correlation time. This correlation time value is not related with any characteristic time of the system dynamics. In fact, it depends on

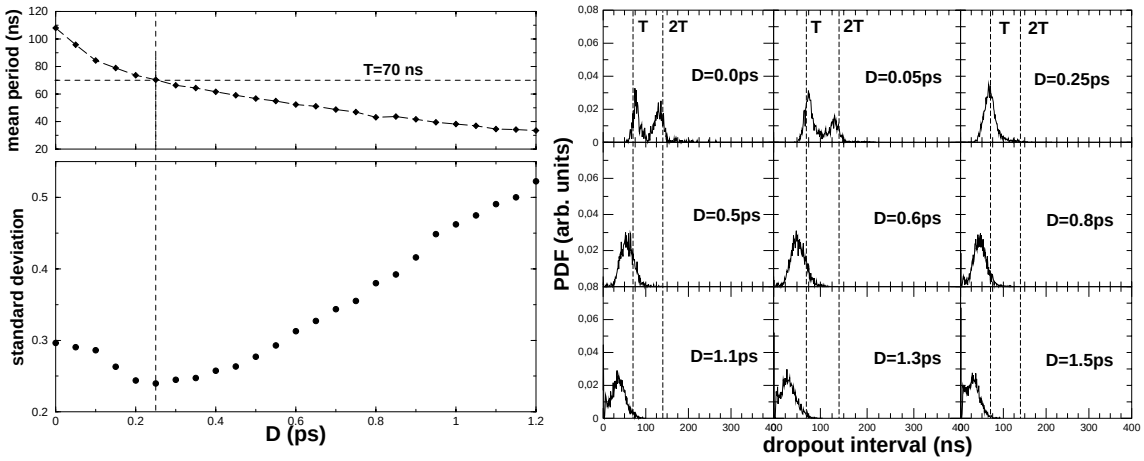

Figure 3. In left figure: mean (top plot) and standard deviation (bottom plot) of the dropout periods for an increasing value of noise intensity D. A minimum located at $D = 0.25$ ps demonstrates that for intermediate values of noise the regularity of the system is maximum. Furthermore, the mean value of the interval between dropouts for the minimum deviation is $t \simeq 70$ ns, which corresponds the period of the modulation. In right figure: Probability distribution functions (PDFs) for increasing values of noise intensity D. It can be seen how the system follows the modulation period when $D = 0.25$ps. When the noise is further increased, the peak observed in the PDF moves to lower intervals between dropouts due to the noise domain in the dynamics.

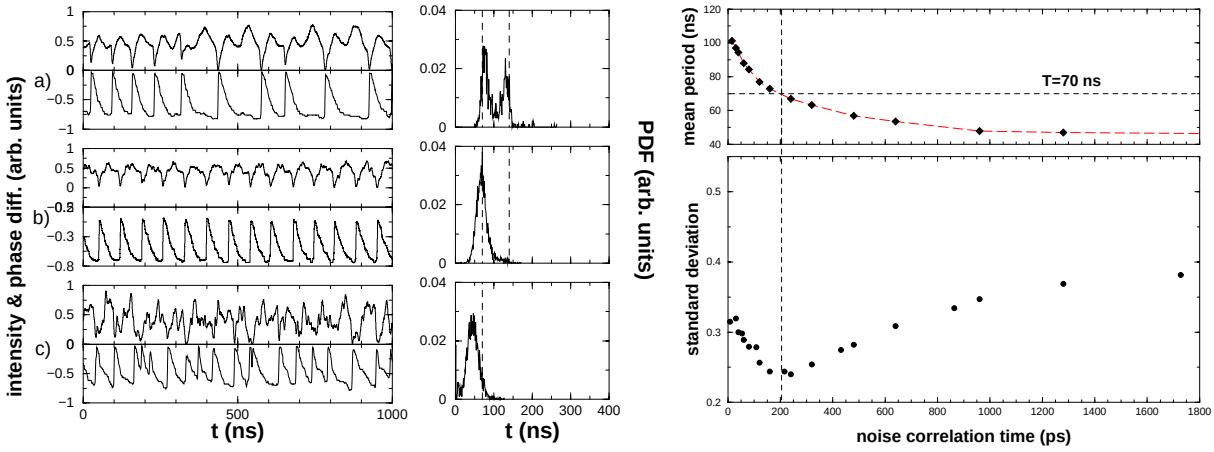

Figure 4. Time evolution of the laser intensity (left column, top plots), the phase difference $\eta(t)$ (left column, bottom plots) and the corresponding PDFs (center column) of the interval between dropouts for increasing values of the external-noise correlation time τ_c: (a) $\tau_c = 15$ ps, (b) $\tau_c = 200$ ps, (c) $\tau_c = 1920$ ps. Note the optimal response of the system to the weak modulation when noise correlation time is increased to $\tau_c = 200$ ps. Noise amplitude is set to $\sigma = 0.035$, modulation amplitude $A = 0.03$ and modulation period $T = 70$ ns. In right column: Mean (top plot) and standard deviation (bottom plot) of the dropout periods for an increasing value of noise correlation time τ_c. A minimum located at $\tau_c \sim 200$ps shows how for intermediate values of noise correlation time, external noise gives the maximum regularity to the interval between dropouts. Furthermore, the mean value of the dropout interval for the minimum deviation is $t \simeq 70$ ns, which corresponds the period of the modulation. Parameters of the simulations are indicated in Appendix A.

the operating conditions of the system, as we will see in the following subsection. We have statistically analyzed the effect of noise correlation for different amounts of noise, observing a variation of the optimal correlation. In this sense, we can conclude that each noise intensity has an optimal correlation time to produce SR.

As in the case of the noise intensity variation, the maximum regularity of the system is also achieved when

the mean period of the dropouts is equal to the modulation period, as it can be seen in Fig. 4. The explanation of this phenomenon is that semiconductor laser carriers play an important role in the dynamics induced by the noise. When high frequency external noise is added to the system the carriers can not follow the fast evolution [see Eq.(2)], and they act as a noise filter. This is the reason why we can not see any effect for low values of the noise correlation time (see Fig. 4). In fact, as the noise correlation time is decreased, we would need to increase the noise amplitude to have similar effects. On the other hand, for low-frequency noise, which means large correlation time ($\sim$ 1 ns), the carriers are able to follow the noise dynamics. It will only be for intermediate values of the noise correlation time, that the system will be assisted by the noise to follow the modulation period.

1.3. Effect of the delay time in stochastic resonance

Let us analyze now the influence of the delay time (τ_f) in the dynamics of the system, and above all, its relation with noise and the SR phenomenon. In Fig. 5 we can see how important is to choose an adequate feedback time (in our case, the external cavity length). We have introduced an external modulation with fixed amplitude and frequency for three different external cavity lengths, always in the absence of noise. In this example it can be observed how the entrainment of the LFF is not achieved for all external cavities. Since it is clear that the feedback time is a significant value in order to obtain an entrainment of the LFF, it is reasonable that τ_f is going to influence in the SR observation. With the aim of observing this phenomenon we have introduced an external noise (with fixed amplitude and correlation time) together with an external periodic signal (also fixed in amplitude and frequency). Under these conditions, we modify the length of the external cavity and therefore the feedback time τ_f.

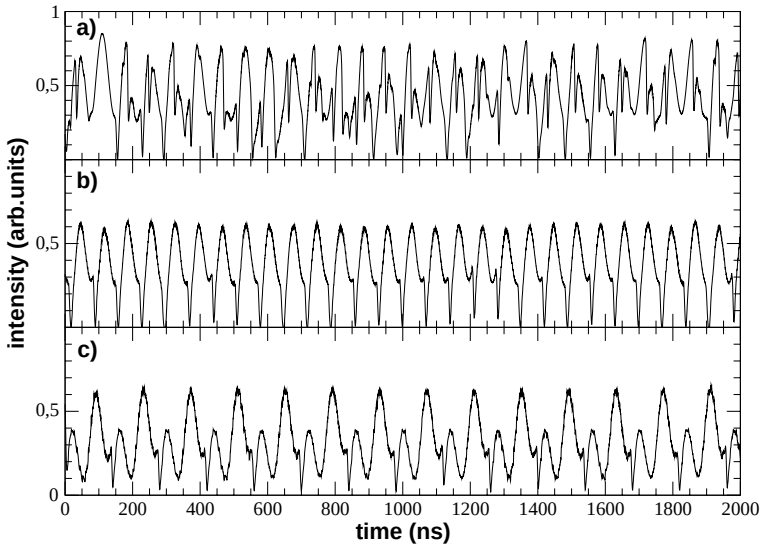

Figure 5. Output intensity for a modulated laser with optical feedback in the LFF regime for different values of the external cavity length τ_f: (a) $\tau_f = 1$ ns, (b) $\tau_f = 2.8$ ns, (c) $\tau_f = 8.4$ ns. We can see that the optimal entrainment is obtained in (b). Modulation period is $T = 70$ ns in all cases, with a fixed amplitude of $A = 0.04 I_{th}$. The rest of the laser parameters are indicated in Appendix A.

In Fig. 6 (top plot) we plot the normalized standard deviation of the interval between dropouts for three different noise levels over a range of external cavity lengths. When noise intensity is increased, the minimum in the standard deviation shifts to higher cavity lengths. In Fig. 6 (bottom plot) we can see how the plateau in the mean interval follows the same trend. This dependence on the cavity length is crucial from the point of view of the SR which cannot be observed equally well for all feedback times. From Fig. 6 (top plot) we can see how SR will not occur at the minima of the solid curve (a), because noise there can only worsen the regularity of the dropouts. The further the operating point is from these minima, the more pronounced the SR effect will be. In Fig. 7, we have plotted the phase difference $\eta(t)$ between the emitted and reinjected fields, exhibiting a pulse when the output intensity has a dropout. We have chosen two different cavity lengths and increased the

noise intensity to observe the SR phenomenon. As expected from the results of Fig. 6 (top plot), SR can not be observed at $\tau_f = 2.8$ ns, where increasing noise destabilizes the regular output of the laser [see Fig. 7(a-c)].

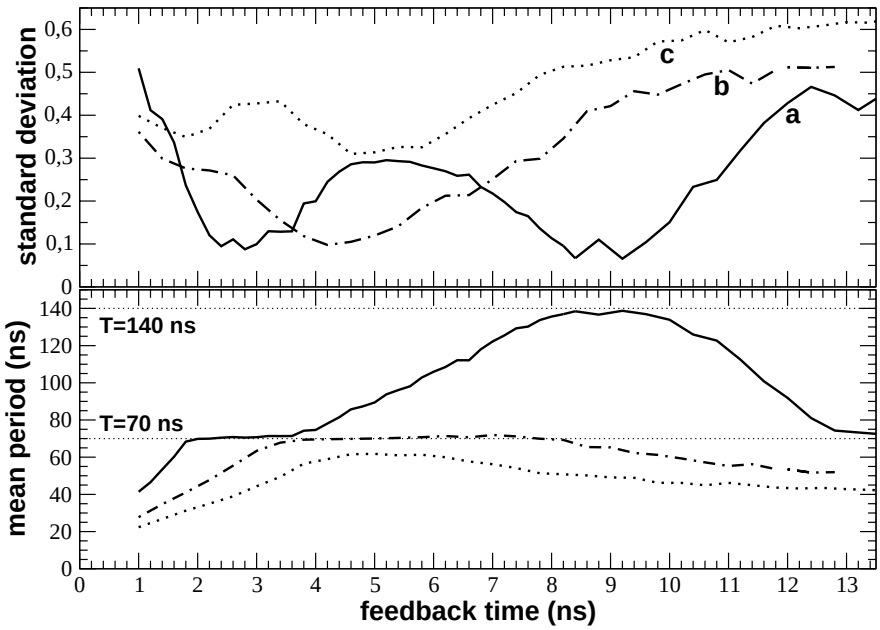

Figure 6. Normalized standard deviation (top plot) and mean period (bottom plot) of the time between dropouts for three different noise amplitudes. $\sigma = 0.00$ for the solid line (a), $\sigma = 0.04$ for the dashed line (b) and $\sigma = 0.06$ for the dotted line (c). In the lower graph, guiding lines indicate the multiples of the modulation period.

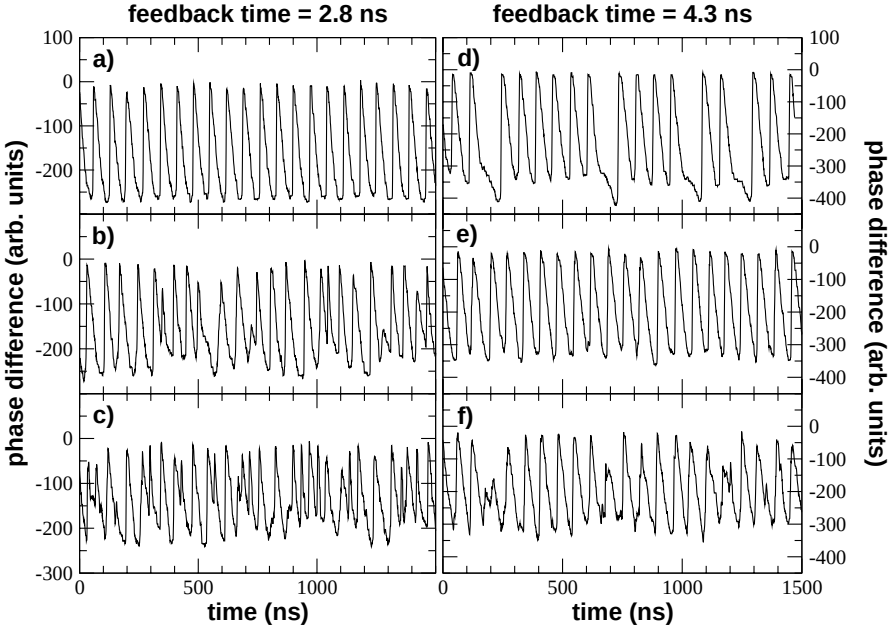

Figure 7. Phase difference for two different cavity lengths. $\tau_f = 2.8$ ns is outside the SR region, and $\tau_f = 4.3$ ns is inside SR region [see Fig. 6 (top plot)]. The values of noise amplitude are: $\sigma = 0.00$ for (a) and (d); $\sigma = 0.025$ for (b) and (e); $\sigma = 0.041$ for (c) and (f). Note that for $\tau_f = 2.8$ ns, noise will disorder the regular output of the laser, while for $\tau_f = 4.3$ ns, intermediate values of noise enhances the regularity of the laser output.

For $\tau_f = 4.3$ ns, we are in the region of SR [see Fig. 6 (top plot)], therefore, intermediate values of noise will increase the regularity of the laser output [see Fig. 7(e)], which is the typical feature of SR.

We can conclude that, although it does not exist a direct relation between the feedback time and the frequency of the external periodic signal, it has an important role in the observation of SR, which can only exists for certain regions of the cavity length.

2. COHERENCE RESONANCE IN SEMICONDUCTOR LASERS

2.1. Noise induces coherence

As we have seen, stochastic resonance consists of an optimization due to noise of the response of a nonlinear system to a weak periodic driving.[21,22] But even in the absence of external periodic forcing, noise can be helpful in sustaining a coherent oscillatory response in the system, provided the operation point is close to a limit cycle[23,24] or within an excitable regime.[25] This phenomenon has been called *coherence resonance* (CR), and has been also found also in bistable,[26,27] chaotic[28] and coupled excitable systems.[29,30]

The first experimental observation of CR in an optical system has been recently made in a semiconductor laser with optical feedback.[31] In that case, noise was added to the driving current of the laser in the absence of any periodic signal, giving rise to a pulsed behavior in the system, in the form of the well known LFF. The regularity of the dropout series initially increased with increasing noise level, and peaked for an optimal amount of noise.

Let us study numerically the CR in our system and how noise can induce coherence by itself. We will use the LK model introduced in the previous section [See Eqs.(1)-(2)] where external modulation is not considered. Since the internal spontaneous-emission noise $\zeta(t)$ cannot be experimentally controlled, we now turn our attention to the effect of the external noise $\xi(t)$ upon the system. This effect can be understood by examining the mechanism behind the previously-mentioned power dropouts, which is well understood in the framework of the LK model (i.e. under the assumption of single-mode operation of the laser). This model exhibits multiple coexisting fixed points, which appear in pairs of solutions called modes and antimodes. The antimodes are saddle points, and most of the modes are also unstable due to a Hopf bifurcation.[32] However, at least one of the modes (the one with maximum power) is stable. In this complex phase-space landscape, a large enough fluctuation may be able to take the system away from the basin of attraction of the stable fixed point and, upon collision with a neighboring antimode, produce a sudden increase in the phase difference which corresponds to a power dropout. Following the dropout, a build-up process begins in which the system undergoes a chaotic itinerancy around the Hopf-unstable modes, jumping consecutively from one to the next while being drifted back towards the stable maximum-gain mode.[33] For small intensities of the external noise, the excursion time t_e required by the system to recover from an intensity dropout is basically independent of noise, and has the role of a refractory time during which no dropouts can be induced. As noise intensity increases the escape events become more frequent, reducing the standard deviation of the interspike intervals accordingly. A minimum of variability occurs for an optimal amount of noise when the dropout separation is of the order of t_e. Beyond that point, noise intensity is large enough to produce escapes before the build-up process is finished (i.e. before the stable mode is reached), which leads to an irregular series of pulses. This sequence of events is depicted in Fig. 8, which shows three time traces of the phase difference between the emitted and reinjected field, $\eta(t)$, for increasing amplitudes of the external noise, keeping its correlation time constant. In this case, the semiconductor laser is biased at 1% above the solitary-laser threshold, a situation for which the system is stable in the absence of external noise. A small amount of noise produces infrequent dropouts [Fig. 8(a)], which become more numerous and regular as the noise amplitude increases [Fig. 8(b)]. For large noise strengths the pulses become increasingly irregular, both in separation and in amplitude [Fig. 8(c)]. Hence, an optimal amplitude of the external noise exists for which the coherence of the pulsed output of the laser is optimal. In order to quantitatively characterize this effect, we compute the standard deviations R_θ and R_μ of the normalized dropout separation $\theta = T/\langle T\rangle$ and normalized dropout amplitude $\mu = A/\langle A\rangle$, respectively,[31] where T is the time interval between two consecutive dropouts, and A is the peak value of the phase difference $\eta(t)$ at a dropout [see Fig. 8(a)], measured with respect to its minimum value between dropouts. The statistical averages are performed over both time and different realizations of the noise. A dropout is detected when the phase difference $\eta(t)$ suddenly increases in a fixed large amount (12π in our case).[15]

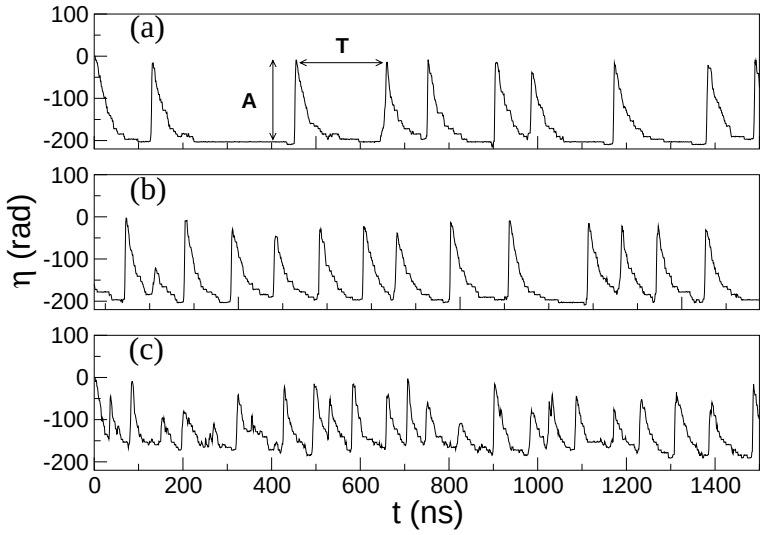

Figure 8. Temporal behavior of the phase difference $\eta(t)$ for increasing noise amplitude: (a) $\sigma = 7.36 \cdot 10^{-2}$, (b) $\sigma = 9.35 \cdot 10^{-2}$, and (c) $\sigma = 1.60 \cdot 10^{-1}$. In all cases we have kept the correlation time constant, $\tau_c = 24$ ps. Other parameters are detailed in Appendix A. In (a), T is the time interval between dropouts and A is the amplitude of the phase difference $\eta(t)$ at a dropout.

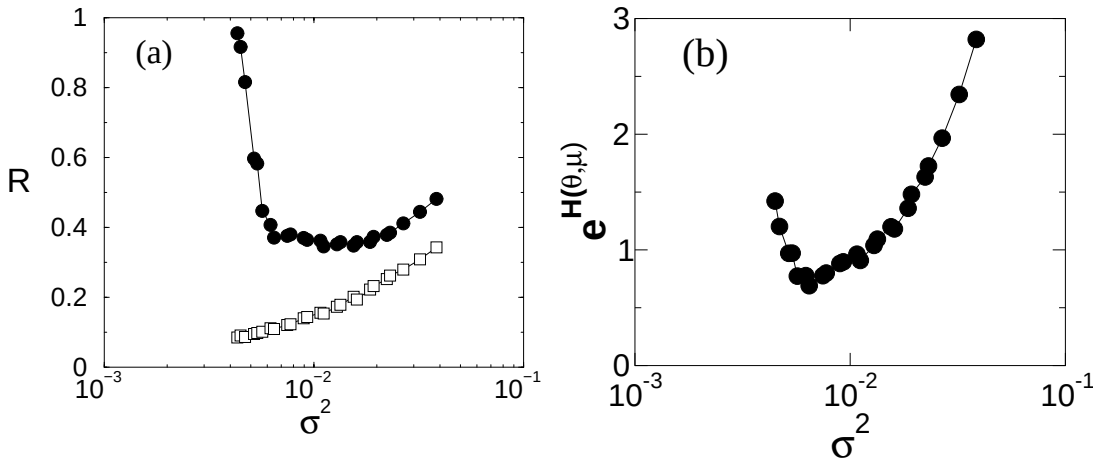

Figure 9. Statistical characterization of the noise-amplitude coherence resonance. (a) Standard deviations R_θ (full circles) and R_μ (empty squares), and (b) joint entropy $H(\theta, \mu)$ as a function of the external noise amplitude. The time correlation of the noise is fixed to $\tau_c = 24$ ps. Other parameters are detailed in Appendix A.

We have computed the standard deviations R_θ and R_μ for increasing noise amplitude, averaging up to 20,000 dropouts in each measure. The result is plotted in Fig. 9(a), and confirms the qualitative conclusions that have been drawn above from Fig. 8, at least as far as the variability of the pulse separation, R_θ, is concerned. This quantity is a non-monotonic function of the noise amplitude, being minimal for an optimal amount of noise. The irregularity of the dropout amplitudes, on the other hand, increases monotonically with noise. This result reflects the fact that the frequency with which noise breaks up the build-up process increases steadily with the amount of noise added.

In order to take into account *both* the dropout separation and amplitude simultaneously in the determination of the signal's regularity, it is useful to define a joint entropy $H(\theta, \mu)$ of the two quantities, where $H = -\sum P \log P$, with P the joint probability density of the two random variables.[34] For the case of two Gaussian independent

random variables the following relation holds[31]: $\exp(H(\theta,\mu)) = 2\pi e R_\theta R_\mu$. We will assume that this result is approximately valid in our case, and compute the joint entropy accordingly. The result is given in Fig. 9(b), which shows again a maximum regularity of the dropout series for an optimal noise amplitude, this time taking into account both the pulse separation and amplitude. In fact, the minimum is in this case more clearly defined.

2.2. Noise correlation time and coherence resonance

We note that all results presented so far have been computed for a fixed correlation time of the noise $\tau_c = 24$ ps, on the order of the fast time scale of the deterministic dynamics.[19] As the white-noise limit is approached the amount of noise necessary to obtain similar effects climbs up to unreasonably high values. As we have discussed in the previous section, the reason is that the carrier dynamics acts as a frequency filter for the external noise [see Eq.(2)], which also prevents the system from responding to high-frequency modulations of the pump current. Therefore, most of the power of a white noise has no effect upon the system dynamics, and the noise intensity needs to be very large in order to have a noticeable influence (a similar effect has been observed in periodic-modulation studies[35]). In the opposite frequency limit a similar situation occurs: for low-frequency forcing the

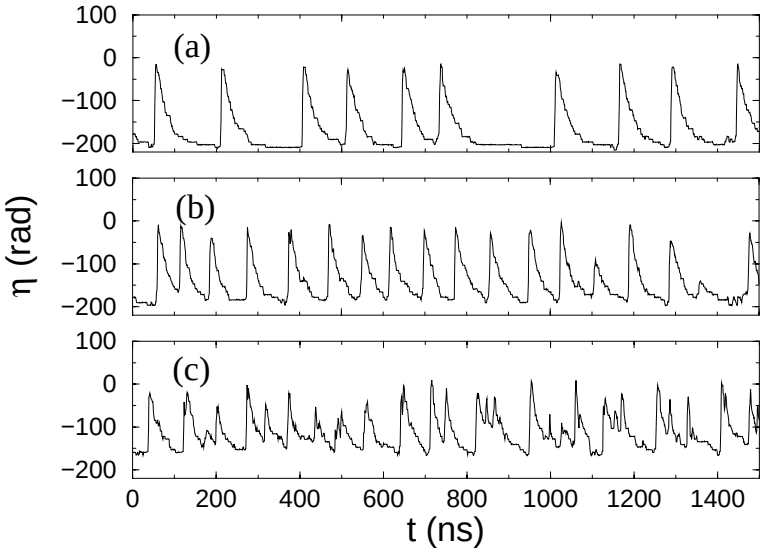

Figure 10. Temporal behavior of the phase difference η for increasing noise correlation time: (a) $\tau_c = 15.8$ ps, (b) $\tau_c = 57.6$ ps, and (c) $\tau_c = 153.2$ ps. In all cases we have kept the noise amplitude constant, $\sigma = 0.079$. Other parameters are detailed in Appendix A.

carrier dynamics has enough time to follow the modulation, and the system responds simply with a modulated output. Only for intermediate frequencies will the external forcing be able to influence the dropout statistics and enhance the coherent response of the system. In order to verify this conjecture, we now fix the amplitude $\sigma = \sqrt{D/\tau_c}$ of the external noise and analyze the behavior of the system for an increasing correlation time of the Ornstein-Uhlenbeck noise defined by Eq.(4). The result is shown in Fig. 10 for three different values of τ_c. It can be seen that the regularity of the pulsed time series improves for intermediate values of the noise correlation time.

We quantify again the qualitative observation made in the previous paragraph by computing the standard deviations R_θ and R_μ, and the joint entropy $H(\theta,\mu)$ of the normalized dropout separation and amplitude. The results, shown in Fig. 11, exhibit the same behavior as in the case of an increasing noise amplitude. Coherence of the pulsed behavior is in this case maximal for a correlation time of the noise $\tau_c \sim 30$ ps. This behavior can be interpreted as a resonance with the fast deterministic dynamics of the system. A similar resonance has been recently observed experimentally in a chemical excitable medium.[36] Nevertheless, it can not be associated to

any characteristic time of the system, since numerical simulations with different noise amplitudes, have shown a maximum coherent response for different values of correlation time.

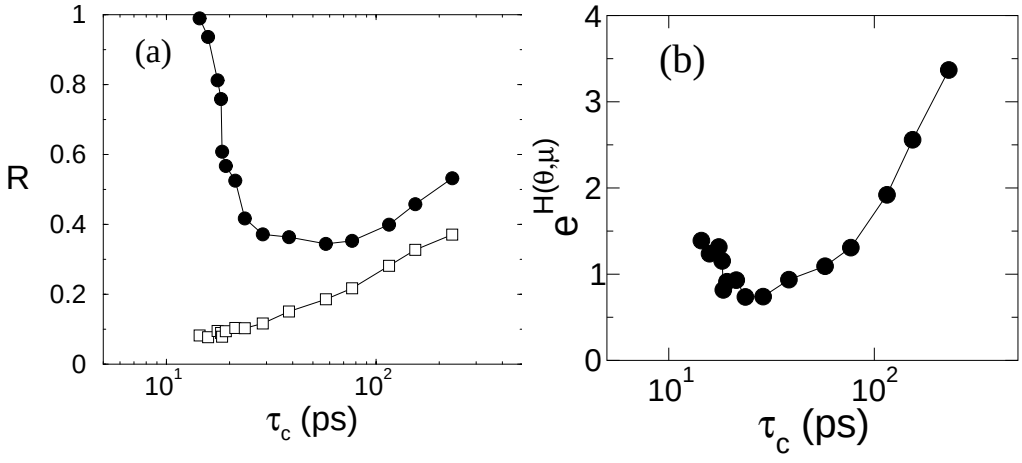

Figure 11. Statistical characterization of the noise-correlation coherence resonance. (a) Standard deviations R_θ (full circles) and R_μ (empty squares), and (b) joint entropy $H(\theta, \mu)$ as a function of the noise correlation time. The noise amplitude is fixed to $\sigma = 0.079$. Other parameters are detailed in Appendix A.

3. GHOST RESONANCE IN SEMICONDUCTOR LASERS

Finally we are going to analyze a recently reported phenomenon, the subharmonic stochastic synchronization,[37] where noise also helps to the entrainment of a nonlinear system when it is externally perturbed by a periodic signal. The main features of this stochastic process are similar to the ones observed in the SR, i.e. entrainment of the system output for certain range of noise amplitude, with the particularity that, in this case, the entrainment is observed at a frequency not present in the periodic input signal. For that reason this phenomenon is also known as ghost resonance (GR).

Firstly we are going to experimentally reproduce the GR in our particular system, a semiconductor laser with optical feedback (in the LFF regime). Secondly we will describe the experimental observation with the LK model [See Eqs.(1)-(2)].

3.1. Experimental results

Our experimental setup shown in Fig. 12, built around an index-guided AlGaInP semiconductor laser (Roithner RLT6505G), with a nominal wavelength of 658 nm. The threshold current is $I_{\rm th} = 18.4$ mA for a temperature of $19.86 \pm 0.01\,^{\rm o}$C. The injection current (IC), without modulation, is set to 19.7 ± 0.1 mA all through the experiment. An antireflection-coated laser-diode objective (L) is used to collimate the emitted light. An external mirror (M) is placed 83.5 cm away from the front facet of the laser, introducing a delay time of $\tau_f \sim 5.56$ ns. The feedback strength is adjusted by placing a neutral density filter (NDF) in the external cavity, which is adjusted so that it yields a threshold reduction of 7.0%. The output intensity is collected by a fast photodetector (PD) and analyzed with a 500 MHz bandwidth acquisition card.

We are interested in the system response to modulation composed of multiple periodic signals $f_1, f_2, ...f_n$. Although the experiment focuses in the case of two components, the driving signal has the following general form[37]:

$$I(t) = I_b \{1 + m [\sin(2\pi(k f_0 t + \Delta f\, t)) + \sin(2\pi((k+1) f_0 t + \Delta f\, t)) + \ldots + \sin(2\pi((k+n-1) f_0 t + \Delta f\, t))]\}, \quad (5)$$

with $k > 1$ and n being the number of external signals of different frequencies. I_b is the bias current and m is the modulation amplitude. Here we choose to use two terms ($n = 2$) and f_0=4.5 MHz (although the same

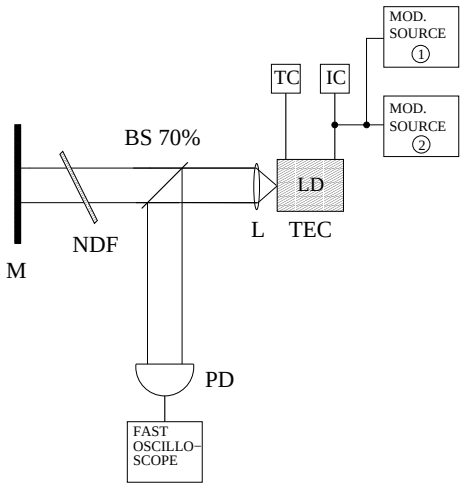

Figure 12. Diagram of the experimental setup: LD, laser diode; BS, beam splitter; TC, Temperature controller; IC, Current source; PD, photodiode; NDF, neutral density filter; M, mirror; L, collimating lens.

qualitative features would be observed for other choices of f_0). For simplicity, initially we describe results for the particular case of $\Delta f = 0$.

The operating parameters of the system are chosen in such a way that in the absence of modulation the laser emits a continuous wave (CW) light intensity. Power dropouts start to appear when a small amount of modulation is added to the laser pump current*. In Fig. 13 we can see the examples of three representative time traces for low ($m = 0.057$), intermediate ($m = 0.0815$) and high ($m = 0.114$) amplitude values of the injected signals. It can be clearly seen that for the intermediate amplitude the dropouts are almost equally spaced at a time interval that corresponds grossly to $1/f_0$ (depicted by the double-headed arrow in the middle panel), a frequency that is not being injected. Thus the laser is detecting in a nonlinear way the subharmonic frequency. To better visualize this fact we plot on the right panels the probability distribution functions (PDF) for a large number of dropouts (approx. 1500). For the small amplitude (top of the center panel) it can be observed a peak at a time $1/f_0$ and other peaks at longer times which indicate that the system responds sometimes to f_0 although at some others times dropouts are skipped. For the optimum value of the amplitude (middle of the center panel) the PDF has a clear peak at $1/f_0$ which indicates that the system is resonating with this frequency. For the higher amplitude (bottom of the center panel) there are several peaks at different times corresponding to higher frequencies.

The resonance with the ghost frequency can be visualized by measuring the mean interval between dropout events and its standard deviation (SD) at various values of the signal amplitude m. Fig. 13 (right panel) shows these results plotted as the normalized SD (i.e., SD/mean) as a function of the mean frequency of dropout events. It is clearly seen that the minimum coincides with the f_0 (vertical dashed line), i.e., the ghost frequency.

The ghost frequency is not, as one naively would expect, simply the difference between the two components f_1 and f_2, (where $f_1 = 2f_0$ and $f_2 = 3f_0$). This is demonstrated by adding a small term (i.e., $\Delta f \neq 0$) which shifts equally both frequencies. In this case we observe that the resonant frequency shifts as well, despite the fact that the difference remains constant. Results from experimental runs using $f_1 = 7$ to 10.5 MHz and $f_2 = 11.5$ to 15 MHz and selecting the optimum amplitude $m = 0.0815$ are presented in Fig. 14 (left plot). The format of the plot is meant to illustrate better the linear change of the resonant frequency f_R as a function of the frequency shift. The PDFs are plotted using frequency (i.e., inverse of the dropout intervals) axis and they are lined up with the f_1 frequency at which were obtained. It can be seen that the density of the most frequent dropouts lies

*In any case, f_0 has been chosen to be larger than the average frequency of the spontaneous dropouts occurring in nearby regions of parameter space, in order to prevent the underlying free-running dynamics of the system from affecting its response to the external signal.

on a straight line. The experimental results show a remarkable agreement with the prediction given in[37] defined by:

$$f_R = f_0 + \frac{\Delta f}{k + 0.5} \tag{6}$$

Since the range of f_1 we explored is about twice f_0, the dotted line labeled 'k=2' predicts the location of the most important resonance and the one 'k=3' the expected ones if the range where to be extended further up. Thus, the results presented in this figure agree extremely well with the ones described previously in a simpler system in[37] and they are the first experimental demonstration of this type of resonance at the ghost frequency.

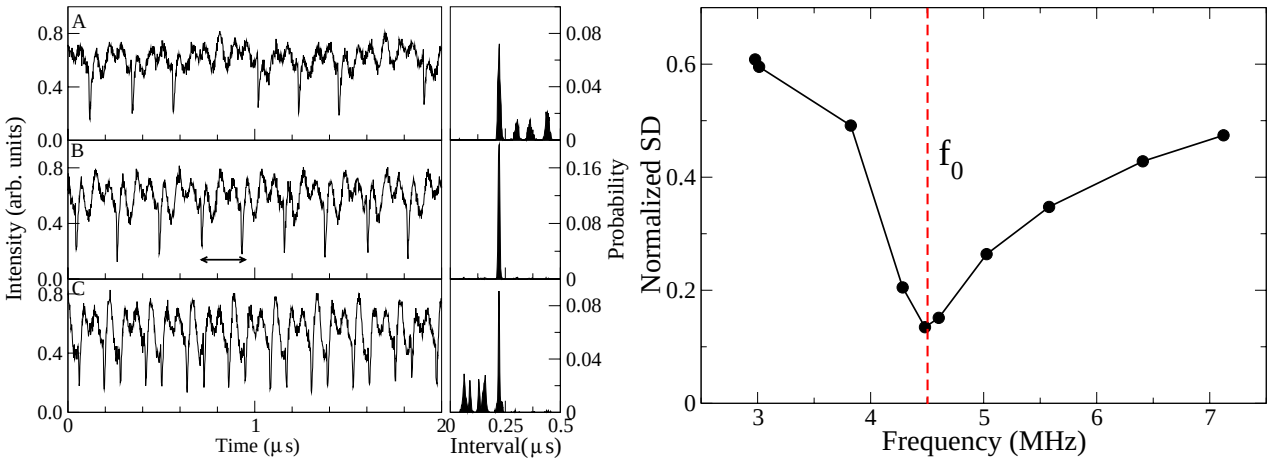

Figure 13. The left panels show the experimental time series for low (A), medium (B) and high (C) injected signals. The center panels depict the PDFs of the dropouts intervals at the three amplitudes. The PDFs largest peak corresponds to $1/f_0$. The right panel shows the standard deviation (SD) of the normalized dropout separation versus the mean frequency between dropouts. The variability of the dropout intervals reaches a minimum when its frequency approaches f_0.

3.2. Numerical results

Finally we have checked that our experimental results can be reproduced by the LK model [See Eqs.(1)-(2)] where the carrier equation [Eq.(2)] has been modified in order to include a term of modulation:

$$\frac{dN}{dt} = C\,(1 + m\{\sin(2\pi(kf_0t + \Delta ft)) + \sin(2\pi((k+1)f_0t + \Delta ft))\}) - \gamma_e\,N(t) - G(|E|^2, N)\,|E(t)|^2 \tag{7}$$

where $\alpha = 3.4$ is the linewidth enhancement factor and $\gamma = 0.24$ ps^{-1} is the cavity decay rate. The feedback strength is set to $\kappa = 20$ ns^{-1} and the external round–trip time to $\tau_f = 5.57$ ns. The laser free running frequency is $\omega/2\pi = 4.56 \times 10^{14}$ Hz. We consider spontaneous emission noise with a rate of ps^{-1}. The first term in Eq.(7) accounts for the injection current with the two sinusoidal inputs at frequencies $2f_0$ and $3f_0$, being $f_0 = 4.5$ MHz and the modulation amplitude $m = 0.0118$ with respect to threshold. $C = 1.26 \times 10^5$ ps^{-1} is the pump parameter, which corresponds to a laser pumped 1.015 times above threshold, with $I_{th} = 19.8$ mA. The rest of the laser parameters are given in Appendix A.

Fig. 14 (right plot) shows the results obtained by numerical simulations. It can be clearly seen that qualitative similar results are obtained as in the experiments, which indicates that the LK model is also able to extract the main features of this new resonant phenomenon. The model also help us to confirm that the experimentally observed behavior is not a simple linear subharmonic resonance.

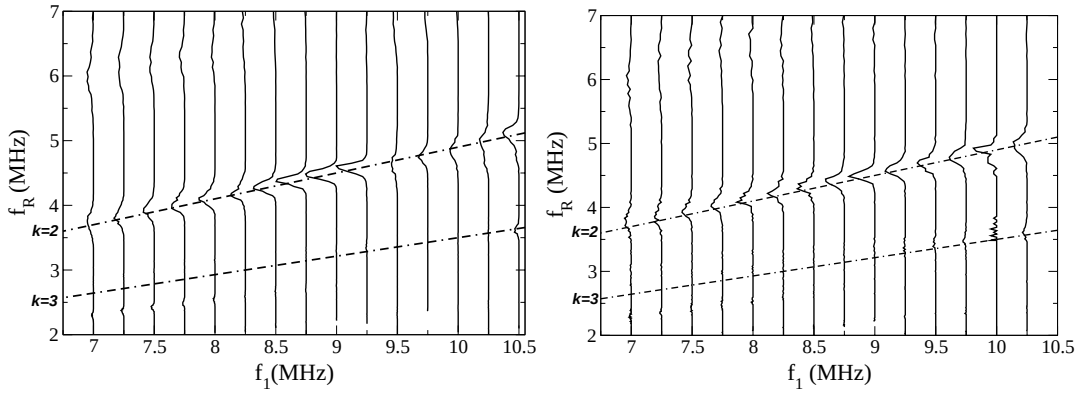

Figure 14. Left plot: Experimental results. PDFs of the intervals between dropouts are plotted as their inverse. For each pair of f_1-f_2 frequencies explored the resulting PDF is plotted at the corresponding f_1 frequency. The guiding lines are theoretical resonance frequencies from Eq.(6). Right plot: Numerical results with the LK model. Laser parameters are indicated in Appendix A.

ACKNOWLEDGMENTS

The authors wolud like to acknowledge financial support from the EU IST network OCCULT IST-2000-29683, from MCyT-FEDER (Spain, projects BFM2002-04369 and BFM2003-07850), and from the Generalitat de Catalunya (project 2001SGR00223).

APPENDIX A. PARAMETERS USED IN THE SIMULATIONS

Symbol	Parameter	Units	Figs.(2,3,4)	Figs.(5,6,7)	Figs.(8,9,10,11)	Fig. (14-b)
C	Normalized pumping current	–	1.03	1.02	1.01	1.015
γ_e	Carrier inverse lifetime	ps^{-1}	$6 \cdot 10^{-4}$	$6 \cdot 10^{-4}$	$6 \cdot 10^{-4}$	$6.2 \cdot 10^{-4}$
γ	Photon inverse lifetime	ps^{-1}	0.158	0.158	0.158	0.24
g_N	Differential gain	ps^{-1}	$2.79 \cdot 10^{-9}$	$2.79 \cdot 10^{-9}$	$2.79 \cdot 10^{-9}$	$2.79 \cdot 10^{-9}$
s	Saturation coefficient	–	$3 \cdot 10^{-7}$	$3 \cdot 10^{-7}$	$3 \cdot 10^{-7}$	$1 \cdot 10^{-7}$
α	Linewidth enhancement factor	–	4.0	5.0	3.5	3.4
N_0	Carrier number at transparency	–	$1.51 \cdot 10^8$	$1.51 \cdot 10^8$	$1.51 \cdot 10^8$	$1.50 \cdot 10^8$
β	Spontaneous emission level	ps^{-1}	$5 \cdot 10^{-10}$	$5 \cdot 10^{-10}$	$5 \cdot 10^{-10}$	$5 \cdot 10^{-10}$
κ	Feedback strength	ps^{-1}	0.025	0.020	0.025	0.020
τ_f	External roundtrip time	ns	2.4	*variable*	2.4	5.57
$\omega\tau_f$	Feedback phase	–	2	0	2	0

Table 1. Laser parameters used in the numerical simulations.

REFERENCES

1. W. Horsthemke and R. Lefever, *Noise-induced transitions*, Springer, Berlin (1984).
2. J. García-Ojalvo and J.M. Sancho, *Noise in Spatially Extended Systems*, Springer, New York (1999).
3. R. Benzi, S. Sutera and A. Vulpiani, *J. Phys. A* **14**, L453 (1981).
4. K. Wiesenfeld and F. Jaramillo, *Chaos* **8**, 539 (1998).
5. A. Longtin, A. Bulsara and F. Moss, *Phys. Rev. Lett.* **67**, 656 (1991).
6. A. Bulsara, E.W. Jacobs, T. Zhou, F. Moss and L.Kiss, *J. Theor. Biol.* **152**, 531 (1991).
7. D.R. Chialvo and A.V. Apkarian, *J. Stat. Phys.* **70**, 375 (1993).

8. S. Fauve and F. Heslot, *Phys. Lett. A* **97**, 5 (1983).
9. G. Debnath, T. Zhou and F. Moss, *Phys. Rev. A* **39**, 4323 (1989).
10. L. Gammaitoni, E. Menichella-Saetta, S. Santucci, F. Marchesoni and C. Presilla, *Phys. Rev. A* **40**, 2114 (1989).
11. B. McNamara, K. Wiesenfeld and R. Roy, *Phys. Rev. Lett.* **60**, 2626 (1988).
12. J. Grohs, S. Apanasevich, P. Jung, H. Ißler, D. Burak and C. Klingshirn, *Phys. Rev. A* **49**, 2199 (1994).
13. R. Bartussek and Peter Hänggi, *Phys. Rev. E* **49**, 3930 (1994).
14. M. Giudici, C. Green, G. Giacomelli, U. Nespolo and J.R. Tredicce, *Phys. Rev. E* **55**, 6414 (1997).
15. J. Mulet and C. R. Mirasso, *Phys. Rev. E* **59**, 5400 (1999).
16. F. Marino, M. Giudici, S. Barland and Salvador Balle, *Phys. Rev. Lett.* **88**, 040601 (2002).
17. R. Lang and K. Kobayashi, *IEEE J. Quantum Electron.* **16**, 347 (1980).
18. I. Fischer, G.H.M. van Tartwijk, A.M. Levine, W. Elsäßer, E. Göbel and D. Lenstra, *Phys. Rev. Lett.* **76**, 220 (1996).
19. D.W. Sukow, T. Heil, I. Fischer, A. Gavrielides, A. Hohl-AbiChedid and W. Elsäßer, *Phys. Rev. A* **60**, 667 (1999).
20. J.M. Buldú, J. García-Ojalvo, C.R. Mirasso, M.C. Torrent and J.M. Sancho, *Phys. Rev. E* **64**, 051109 (2001).
21. K. Wiesenfeld and F. Moss, *Nature* **373**, 33 (1995).
22. L. Gammaitoni, P. Hänggi, P. Jung and F. Marchesoni, *Rev. Mod. Phys.* **70**, 223 (1998).
23. H. Gang, T. Ditzinger, C.Z. Ning and H. Haken, *Phys. Rev. Lett.* **71**, 807 (1993).
24. W.J. Rappel and S.H. Strogatz, *Phys. Rev. E* **50**, 3249 (1994).
25. A.S. Pikovsky and J. Kurths, *Phys. Rev. Lett.* **78**, 775 (1997).
26. B. Lindner and L. Schimansky-Geier, *Phys. Rev. E* **61**, 6103 (2000).
27. A. Zaikin, J. García-Ojalvo, R. Báscones, E. Ullner and J. Kurths, *Phys. Rev. Lett.* **90**, 030601 (2003).
28. C. Palenzuela, R. Toral, C. Mirasso, O. Calvo and J. Gunton, *Europhys. Lett.* **56**, 347 (2001).
29. H. Hempel, L. Schimansky-Geier and J. García-Ojalvo, *Phys. Rev. Lett.* **82**, 3713 (1999).
30. S.K. Han, T.G. Yim, D.E. Postnov and O.V. Sosnovseva, *Phys. Rev. Lett.* **83**, 1771 (1999).
31. G. Giacomelli, M. Giudici, S. Balle and J.R. Tredicce, *Phys. Rev. Lett.* **84**, 3298 (2000).
32. A.M. Levine, G.H.M. van Tartwijk, D. Lenstra, and T. Erneux, *Phys. Rev. A* **52**, R3436 (1995).
33. T. Sano, *Phys. Rev. A* **50**, 2719 (1994).
34. R. Badii and P. Politi, *Complexity: hierarchical structures and scaling in physics*, Cambridge University Press, Cambridge (1997).
35. D.W. Sukow and D.J. Gauthier, *IEEE J. Quantum Electron.* **36**, 175 (2000).
36. I. Sendiña-Nadal, S. Alonso, V. Pérez-Muñuzuri, M. Gómez-Gesteira, V. Pérez-Villar, L. Ramírez-Piscina, J. Casademunt, J. M. Sancho, and F. Sagués, *Phys. Rev. Lett.* **84**, 2734 (2000).
37. D. R. Chialvo, O. Calvo, D.L. Gonzalez, O. Piro and G.V. Savino, *Phys. Rev. E* **65** 050902 (2002).